Non-invasive density and porosity fraction mapping of bituminous coal using ultrasound *⊙*

Yuqi Jin 💿 ; Teng Yang 💿 ; Menglin Yao 💿 ; Zhiming Wang 💿 ; Narendra B. Dahotre 📵 ; Arup Neogi 🗷 📵



J. Appl. Phys. 134, 075105 (2023) https://doi.org/10.1063/5.0161877





CrossMark

Articles You May Be Interested In

Strength properties of polyethylene in bituminous mixtures for flexible pavement

AIP Conference Proceedings (November 2018)

The application of mathematical methods in the development of bituminous binders with the required operation interval

AIP Conference Proceedings (July 2023)

Plastic waste bituminous concrete for a sustainable waste management approach

AIP Conf. Proc. (September 2019)

500 kHz or 8.5 GHz? And all the ranges in between.

Lock-in Amplifiers for your periodic signal measurements









2023 19:36:26

Non-invasive density and porosity fraction mapping of bituminous coal using ultrasound

Cite as: J. Appl. Phys. 134, 075105 (2023); doi: 10.1063/5.0161877

Submitted: 12 June 2023 · Accepted: 26 July 2023 ·

Published Online: 21 August 2023







Yuqi Jin, 🖟 Teng Yang, 🎾 Menglin Yao, 🕉 🕩 Zhiming Wang, 🗘 🕩 Narendra B. Dahotre, 🗘 🕩 and Arup Neogi 🗀 🕩

AFFILIATIONS

- ¹Department of Physics, University of North Texas, Denton, Texas 76207, USA
- ²Department of Materials Science and Engineering, University of North Texas, Denton, Texas 76207, USA
- ³Institute of Fundamental and Frontier Sciences, University of Electronic Science and Technology of China, Chengdu 611731, People's Republic of China

ABSTRACT

The principle of the conventional ultrasound test states that the detectable voids cannot be smaller than the acoustic wavelength. However, by using effective medium approximation, the fraction of small voids can be estimated by the variation of the effective density. In this study, a non-contacting ultrasound-based porosity fraction mapping methodology is developed for estimated small voids in coal with long operating wavelength in air. This novel ultrasonic technique based on the mechanical properties of coal offers a rapid scan of the effective density mapping and distribution of void fraction over a large sample area, which overcame the limitation of small voids detection in the conventional ultrasound testing.

Published under an exclusive license by AIP Publishing, https://doi.org/10.1063/5.0161877

I. INTRODUCTION

Coal is still a major energy source with vastly different energy efficiencies dependent on the coal mines' geological location and environmental conditions. It is necessary to characterize the porosity of the coals embedded within a mine to evaluate its energy efficiency and rate the quality of the coal. The difference in coal's porosity leads to varying behaviors in coal bed methane and the overall performance of the power generation.² In the various coal systems, the quality of coal can be rated based on the average size of the pores,³ including micropores, mesopores, and macropores. In general, the average porosity size can be observed by microscopic methods. However, the porosity distribution is highly non-uniform in organic and inorganic coals.5 Atomic force microscopy and x rays were applied to evaluate the porosity distributions and sizes related to the gas absorption and mechanical failure phenomenon.6 The performance of the electromagnetic or radiational evaluation techniques is efficient and widely used. However, due to its short operating wavelength, electromagnetic testing methods are limited to coal samples with small testing sizes. As an alternative method, a novel non-invasive porosity distribution mapping method is proposed using in-air ultrasound techniques in the present work.

Ultrasound is broadly used in biomedical⁷ and industrial^{8,9} areas due to its excellent penetration compared to electromagnetic or radiational characterization methods. The propagation of ultrasound is highly sensitive to the existence of discontinuity, such as pores or defects in the rock with voids or trapped gases. A sharp variation in the mechanical property at the interfaces between the porosity and its surrounding region introduces a mismatch in the acoustic impedances proportional to density and sound velocity. The acoustic impedance mismatch at the porosity-surrounding interface separates the acoustic energy into transmission and reflection modes in a normal incidence configuration for a comparable or larger porosity relative to the operating acoustic wavelength. Based on detecting the change in the reflected intensity of sound, this principle is the foundation of nondestructive ultrasound testing 10 and medical ultrasound imaging.¹¹ However, when the porosity size is much smaller than the acoustic wavelength, the reflected acoustic wave can be weak due to the complex transmission and scattering of the acoustic waves within the medium. From the view of the acoustic wave, the propagated medium and its porosity are homogenized to an effective uniform material, as the effective medium theory describes. 12 This phenomenon leads to an effective variation of the physical properties based on the mechanical properties and volumetric fraction of the internal

a)Author to whom correspondence should be addressed: arupn@yahoo.com

porosity that can be sensed by a wave propagating through the medium. The effectively modified physical properties of the medium change the propagation of the acoustic wave in terms of its time-of-flight and acoustic pressure amplitude. Based on this principle, in this study, the ultrasound porosity fraction mapping is obtained from the calculation based on the ultrasonic effective density maps ^{13,14} with an effective medium theory.

II. NUMERICAL SIMULATIONS

The effect on acoustic wave propagation through coal in the presence of small pores was analyzed from a numerical model. The numerical simulations were conducted to parameterize the effect of the single pore size and the dependence of the porosity fraction on the time-of-flight amplitude of the acoustic signal propagating through the coal sample. The numerical simulations were performed using the time-domain pressure wave module 15,16 in COMSOL Multiphysics 5.5, a finite element analysis software. Noted that pressure wave module eliminated the presence of shear modes. The selection on this module was due to the difficulty in the convergence in elastic wave module when the solid/air interface presence. Hence, the estimation of the effective density might be underestimated from the pressure wave approach in terms of the absolute value. But the contrast in each mapping should remain comparable. Figure 1(a) illustrates that an active transducer was attached to a rectangular background air domain. A lump of rectangular coal is located at the farther edge relative to the transducer's location in an air medium. The acoustic property of the coal was obtained from the existing literature.¹⁷ The material of the transducer is set to air relative to the background air domain for a cleaner time-domain signal. The interface between the transducer and air domain is perfectly matched. A boundary probe for time-dependent acoustic pressure detection is located at the interface between the transducer and background air. In the porosity size study, only one small pore at the center of the coal along the wave propagation direction is located. The pore sizes were selected to 0.01\(\lambda\), 0.05\(\lambda\), 0.1\(\lambda\), 0.15\(\lambda\), 0.2λ , and 0.25λ , where λ refers to the operating wavelength of the sound wave. For estimating the effect of the filling fraction (F), the size of the pores was set to 0.01 λ, and by increasing the number of the pores, the gas fraction varies as 0.0006, 0.016, 0.064, 0.143, 0.254, and 0.396. In the numerical model, the lower boundary edge was set to sound hard boundary for a complete reflection to represent the large impedance mismatch between ambient air and metal table surface in future experiments. The other outer boundaries were set to the air impedance to avoid the sidewall diffractions. The acoustic source was a causal pulse whose inward velocity was expressed as $\sin(\omega_0 t)e^{-f_0(t-3T_0)^2}$, where ω_0 was the angular frequency of the pulse at the center frequency $f_0 = 1 \text{ MHz}$, and T_0 was the inverse of the f_0 . t refers to the studied time points. The time window's full length was set to 80 T_0 for all the cases.

At t_1 , the transducer emits a short acoustic pulse propagating in the air domain, forwarding to the coal with a width approximately comparable with the width of the transducer. At the interface between the upper surface of coal and the background air domain, the source pulse separates into the transmission with continuous propagation and a reflected echo back to the location of the transducer, as the time point t_2 [Fig. 1(c)] indicates. At t_3 , the acoustic

pulse passes through the pore inside the coal. Due to the relatively slower sound velocity and much lower density of the air pore relative to the coal, the center of the acoustic pulse envelope shows a strong temporal delay and weakened pulse amplitude [Fig. 1(d)]. Figure 1(e) shows the additional echo is excited from the internal pore after the source pulse passes through with low amplitude at t_4 . The central low-pressure region on the pulse envelope (t_3) is slightly recovered at t_4 due to the spatial dispersion effect on the acoustic pulse. Figure 1(f) shows the acoustic pulse reflects at the upper boundary without energy loss and propagates back to the location of the transducer.

Figure 2(a) summarizes the results from the parametric study on the size of a single air pore in coal. In the contour, it is obvious to capture two major reflections around 37 and 50 µs which occurred from the upper surface and the lower surface of the coal domain. In summary, the first reflections (37 μ s) are identical in all the studied cases due to the identical medium the pulse propagated before the pulse arrives at the location of the pore. On the contrary, the second reflections are not indistinguishable due to the propagation back and forth through the pore and traversing the voids twice. Figure 2(b) shows the zoomed-in view of the second reflection signal. The amplitude of the signal shows a slight decrease along with the increase of the pore diameter. The variance in the time-of-flight of the reflection is not distinctly observed. An additional reflection excited from the pore is not visible under the color scale in Fig. 2(a) between the first and the second reflection signal. In Fig. 2(c), the time range 41 to $45 \mu s$ is, therefore, plotted separately with a color scale for the smaller acoustic pressure range. With the increase in the pore size, the amplitude of the additional shows a sharp increase with a strong transition at $d = 0.15 \lambda$. Rowever, these additional reflections [Fig. 2(c)] generally reduce the acoustic pressure to three orders of magnitude lower than the first reflection [Fig. 2(a)]. Experimental detection might not be feasible.

Figure 2(d) summarizes the porosity fraction-dependent parametric study from the further numerical simulations (red line). Based on the first and second reflections from the upper and lower boundaries of the coal, the effective density ρ_{eff} of the coal can be estimated by Eq. (1):^{13,18}

$$\rho_{eff} = c^{-1} Z_0 \left(\frac{-1 - \beta - \sqrt{4\beta + 1}}{\beta - 2} \right), \quad \frac{Z}{Z_0} > 1,$$
(1)

where dimensionless factor $\beta = \frac{p_1}{p_e - p_0}$, p_e is the magnitude of the source pulse from the transducer, p_0 and p_1 are the magnitude of reflection from the upper and lower surface of the coal, c is the speed of sound in the sample, Z is the acoustic impedance of the scanned sample, and Z_0 is the reference acoustic impedance of the ambient medium (air in this study).

The estimated effective density values from the ultrasound reflections compared to the theoretical values (blue line) showed good agreement. The theoretical values were obtained from the effective medium approximation theory, 12 which is expressed as

$$\rho_{eff} = \rho_{coal} \sqrt{1 - F}, \tag{2}$$

where ρ_{coal} refers to the density of coal without voids and F indicates the void fraction.

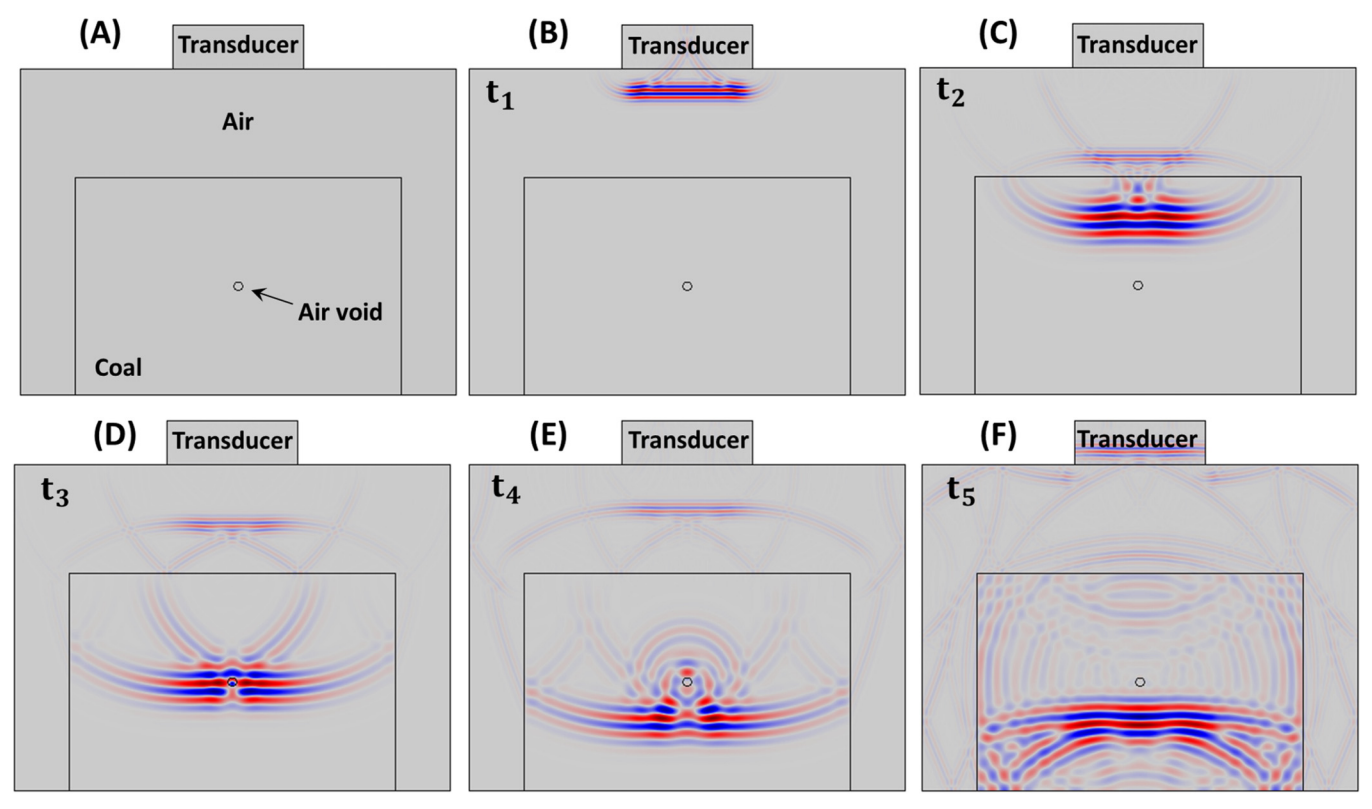


FIG. 1. Study configuration and numerical simulation. (a) The illustration on the monostatic configuration of the numerical simulation models in the time-domain acoustic wave propagation models. (b)—(f) Example of acoustic wave propagation during the ultrasound testing in air. The time points follow $t_1 < t_2 < t_3 < t_4 < t_5$. (b) The excitation of a short acoustic pulse from the transducer. (c) The source pulse separated into transmission and reflection at the interface between air and coal. (d) The transmitted pulse is propagating through the internal pore. (e) A minor reflection is excited by the internal pore. (f) The transmitted pulse reflected back at the lower boundary of the coal.

In the ideal cases, such as the simulation environment, the ultrasound evaluated effective density values are highly mismatched with the effective medium theory. The slight differences were attributed to the presence of the additional reflection from the pores, as illustrated in Fig. 1. As size dependent study demonstrated, with the operating wavelength approaching the size of the pore, higher amplitude additional reflections are expected from the pores, which leads to a larger uncertainty of the second major reflection for the calculation by Eq. (1). However, the operating wavelength can be considered as a variable dependent on the volume fraction of the porosity as the expression $1/\lambda_{eff} = F/\lambda_{air} + (1 - F)/\lambda_{coal}$ described in Ref. 12, where F being the porosity factor or the filling fraction of the composite. In the inset shown in Fig. 2(d), the behavior of the effective operating wavelength was calculated relative to the porosity fraction. With the increase of the porosity fraction, the decreased effective wavelength approached the porosity's size, inducing stronger additional reflection from the pores. Hence, from the comparison shown in Fig. 2(d), the difference between the red and blue lines increases along the increased porosity fraction.

For applying the effective medium approximation, the air void sizes in the sample need to be much smaller than the operating

wavelength. Then, the mechanical properties between the small void and the surrounding material need to have clear differences. Among the different types of effective medium approximation, the one selected in this study was more suitable for strong mechanical property contrast, such as solid and gas. When the proposed methodology was applied to other materials' environment with weaker contrast, the selected effective medium approximation can be replaced by other effective medium approximation theories.

III. EXPERIMENT ON THE BITUMINOUS COAL SAMPLE

The effective density mapping was conducted in the air ambient on a metal table with the ultrasound transducer above the tested sample indicated in Fig. 3(a). An Ultran group, NCG1-D25 1-in. diameter 1 MHz transducer, was equipped to excite a broadband pulse at a repetition rate of 100 Hz. The mapping was realized by a raster scan controlled by MATLAB® script-defined translation motion for the UR5 robotic arm. A JSR Ultrasonic DPR 500 Pulse/Receiver offered the broadband pulse source. The reflection signals were acquired by a Tektronix MDO 304 oscilloscope at a 1 GHz sampling rate in the time domain with a lowpass filter at 5 MHz.

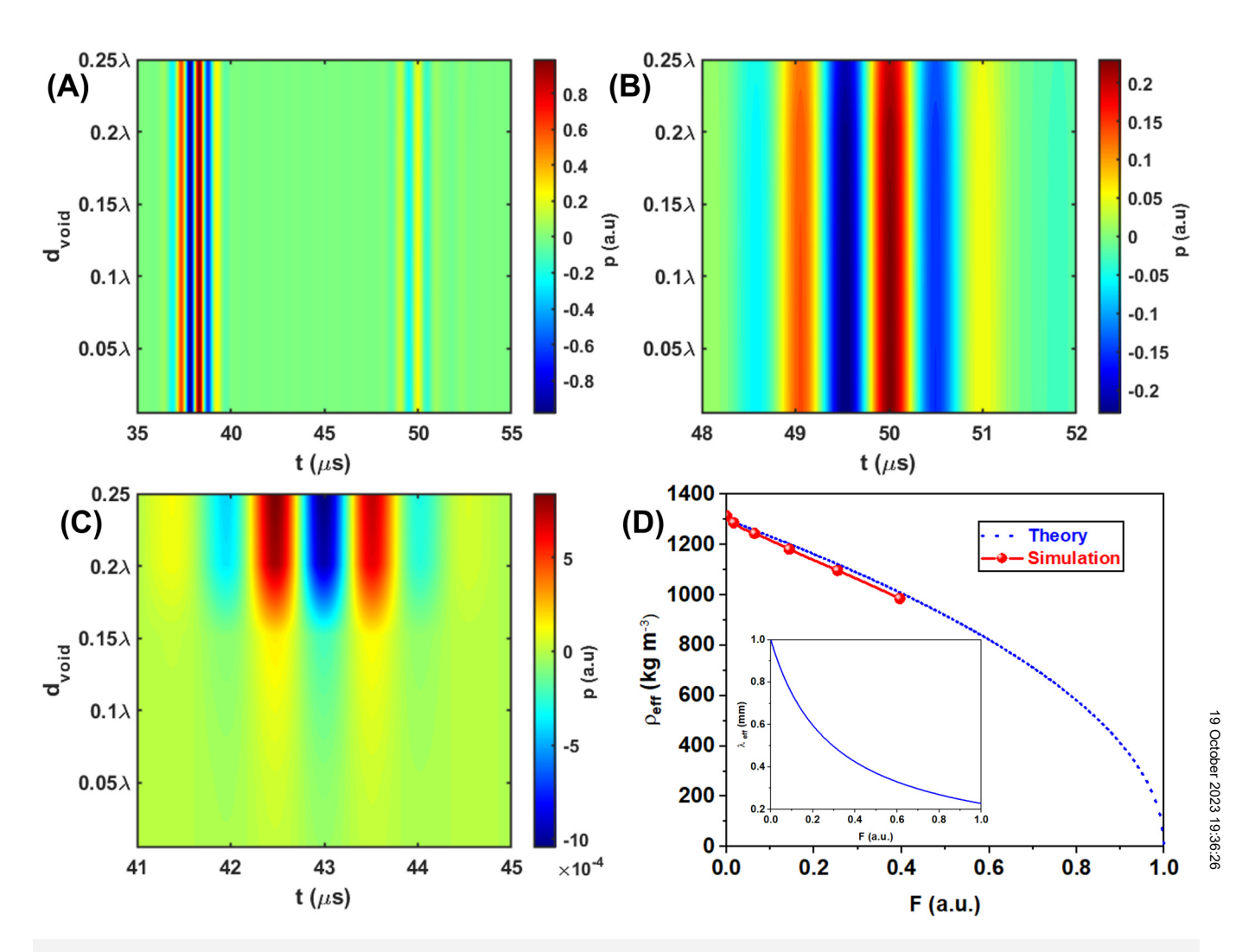


FIG. 2. Simulation results. (a) The combination of the time-of-flight signals on the studied testing configuration with different sizes of a single pore in coal. (b) Zoomed-in view from (a) at the second major reflection from the lower boundary of the coal. (c) Zoomed-in view between the first and second major reflections shows the additional echo from the pore, whose amplitude is highly dependent on the ratio between pore size and operating wavelength. (d) Estimated effective density values (red line) from ultrasound reflections in the parametric study of varying porosity fraction (f). The results are compared to the theoretically calculated effect density values using the effective medium theory. The inset shows the effective wavelength behavior with the increase in the porosity fraction.

The raster-scanned area was 50 by 50 mm with 1 mm spatial intervals. At each scanned location, the motion of the scan was paused for the averaging processes of the collected acoustic signal with 512 signals in the oscilloscope. The bituminous coal sample [Fig. 3(b)] was purchased from Amazon.com.

Figure 3(c) shows the effective density map obtained from the experimental experimentally recorded first and second reflections from the coal sample using Eq. (1). The effective density map presents a highly comparable geometry that can be correlated to the actual photograph in Fig. 3(b). The size of the coal mapped in the effective density map was enlarged around 1–2 mm compared to the actual size due to the finite acoustic beam size. From the air ambient scanned in the map, the values were overestimated to

around $350 \,\mathrm{kg}\,\mathrm{m}^{-3}$ due to the lack of the first reflection in the ambient air. In the coal region, the values are meaningful because both major reflections from the upper and lower surfaces exist. Around the boundary between the coal and surrounding air, the faded-out interface is caused by the smaller scan interval step compared with the acoustic beam size. The estimated effective density of the scanned coal is in the range of around 984 to $1250 \,\mathrm{kg}\,\mathrm{m}^{-3}$ within the reasonable range compared with the density values from the existing literature measured by other techniques. ¹⁹ The horizontal width (on the XY plane) does not affect the acoustic wave propagation, which is along the Z axis. Hence, noted that the low gas fraction regions did not correspond to the widest sections of the coal sample. Figure 3(c) has been performed by high spatial

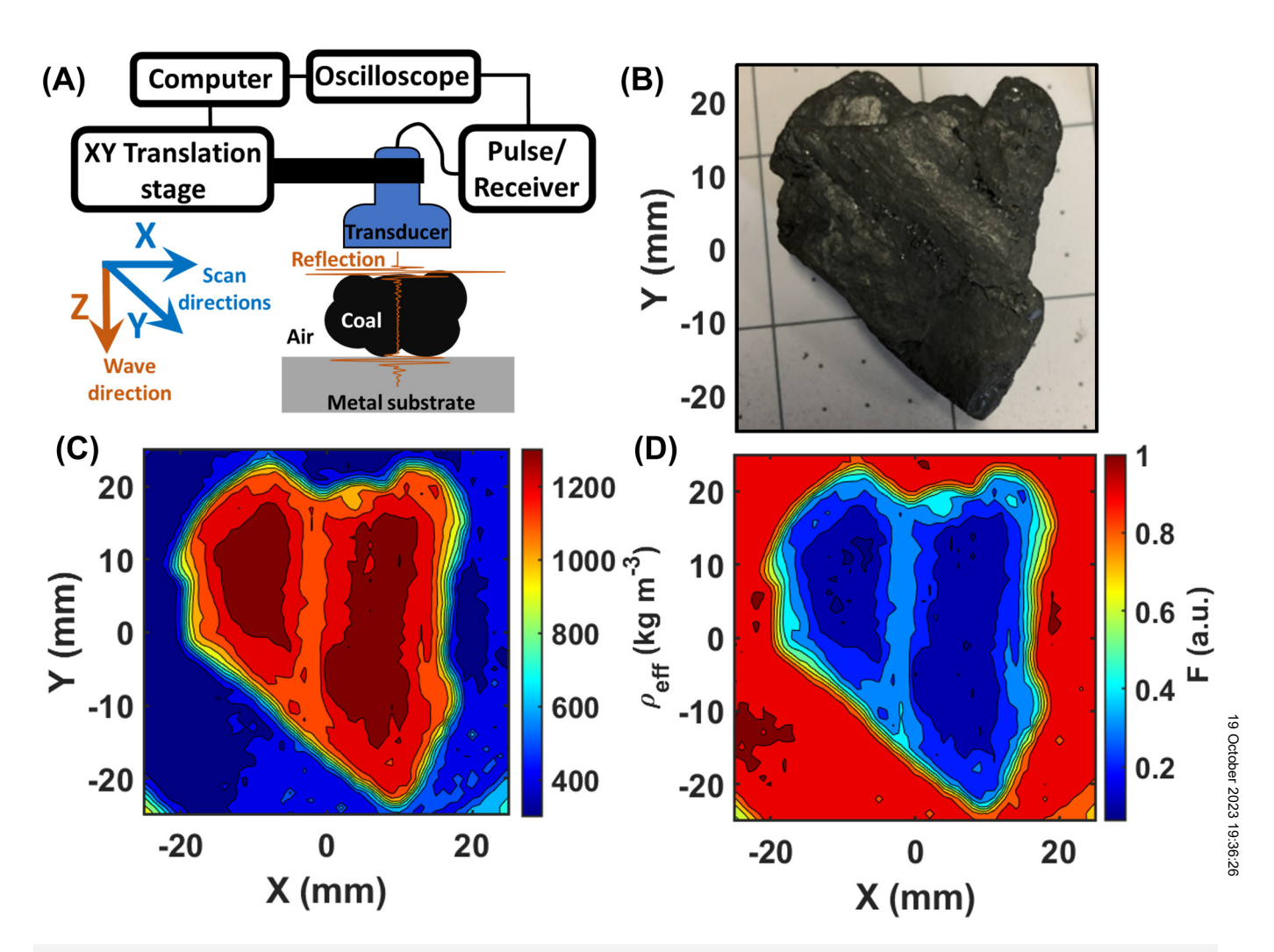


FIG. 3. Experimental scan on a bituminous coal sample. (a) Experimental setup. (b) Photograph of the scanned sample and the scanned area. (c) Effective density map from the two major reflections from the upper and lower boundary of the coal sample. (d) Calculated porosity fraction map based on the map in (c) using effective medium theory.

resolution at 1 mm interval on both X and Y axes. The total time for obtaining the map was about 3.5 h. In practical use of the proposed methodology, decreasing the spatial resolution by increasing the step interval can significantly shorten the time cost of conducting one set of effective density map and void fraction map.

The distribution of effective density showed two denser regions vertically arranged on the sample, which is not comparable to the geometric texture shown in the photograph, which indicated that the surface roughness and geometry do not heavily influence the effective density value measurement. Equation (2) was used to translate the effective density map to a porosity volumetric fraction map based on the assumption of the existence of the gaseous material in pores [Fig. 3(d)]. The fraction map illustrates 100% gas fraction on the surrounding air ambient, which is more reasonable when compared to the effective density map. Furthermore, the

uniformity of the ambient air region is distinctly enhanced in Fig. 3(d) when compared to the inset in Fig. 3(c) (effective density map). On the coal, the fractional map showed more details which agrees with the general distribution of the effective density map. From the exclusive boundary between the coal and surrounding, the estimated gas volumetric fraction is in the range of 0.13–0.31.

Noted that, it was possible that methane gas was also trapped inside of the voids in the coal samples. Based on the acoustic impedance mismatch condition, both air (1.3 kg m⁻³) and methane (0.7 kg m⁻³) provide impedance mismatching condition beyond 99% with the solid part of the coal (1000+ kg m⁻³). Hence, the existence of organic gas voids was considered to provide negligible impact on the estimation of the void fraction mapping. On the contrary, the proposed method on its current stage is not able to distinguish air voids and other organic gas voids. Some direct

relationships such as power laws that express the relationship between physical properties sound wave behaviors would be useful to obtain in the future studies. First, due to the assumption of small voids and the experimental absence of the internal echo, the major contribution of the acoustic attenuation from the voids is induced by Rayleigh scattering that provides the relationship between acoustic attenuation and the operating wavelength as $\alpha \propto f^4$. In addition, dispersion induced pulse elongation can be another target to find which is results by the fraction deviation of voids. Such relationships can be the study target in the future via experimental approaches with constant thickness samples.

One major limitation of the proposed method is the geometry of the target sample. On the transversal plane, geometry is not important for the proposed method. However, the thickness deviation (along the wave propagation direction) of the sample should be remained within one operating wavelength. In simulation, the rectangular setup can exclude uncertainty on the contrast of the void fraction determination, that makes the numerical results can be compared with theoretical estimation. In practical, the incidence wave needs to be normal direction with respect to the metal table under the tested samples. Between the sample upper surface and the metal table, the scanned volume is an approximate cube. The tested sample is not necessary to be flat or rectangular. Another major limitation is the impedance mismatch between the ambient air and tested material. For testing metal for hard ceramic materials, underwater environment can replace the air ambient for reducing the impedance mismatching between the sample and ambient. The unsuitable applications are proposed to the composite materials with high complexity on the compositions and geometry. In future study, the verification of the proposed methodology needs to be performed by a conventional and nondestructive method, such as 3D CT mapping. And, the correlation between the ultrasound approach and conventional approach needs to be connected in not only relative scale [Fig. 3(d)] but also the absolute values.

IV. CONCLUSIONS

In the present study, a novel ultrasound mapping technique was introduced to provide the distribution of the gas pore fraction on coal material based on mapping the effective density distribution with a large testing size and fast. The methodology showed the feasibility to map the distribution of the gas voids that have much smaller size with respect to the operating wavelength. The proposed theory was initially verified by using acoustic wave numerical simulations. In the models, the acoustic wave behavior was determined from the parametric study in a single void's size. From the numerical parametric study in porosity fraction-dependent effective density estimation, the accuracy of the proposed method was compared with the theoretically calculated values from the conventional effective medium theory showing small uncertainty. The small uncertainty in the proposed method was then discovered due to the gas fraction-dependent effective wavelength variation. Finally, the mapping experiment was demonstrated on a relatively flat bituminous coal sample to obtain an effective density map and gas fraction map. The obtained effective density values on the map are located in the reason range with respect to the density range of bituminous coal in the existing literature.

ACKNOWLEDGMENTS

This work was supported by an Emerging Frontiers in Research and Innovation (EFRI) grant from the National Science Foundation (NSF; Grant No. 1741677). Arup Neogi also acknowledges the support from the Distinguished Professorship start-up funds from UESTC and Ministry of Science and Technology of (MOST) International Collaboration Grant 2022YFE0129000 entitled "Cavity Acoustodynamics for nonreciprocal wave propagation."

AUTHOR DECLARATIONS

Conflict of Interest

The authors have no conflicts to disclose.

Author Contributions

Yuqi Jin: Data curation (equal); Formal analysis (equal); Methodology (equal); Writing - original draft (equal). Teng Yang: Data curation (equal); Formal analysis (equal); Methodology (equal); Validation (equal); Visualization (equal); Writing - original draft (equal). Menglin Yao: Validation (equal); Visualization (equal); Writing - original draft (equal); Writing - review & editing (equal). Zhiming Wang: Investigation (equal); Project administration (equal); Supervision (equal); Writing - review & editing (equal). Narendra B. Dahotre: Project administration (equal); Supervision (equal); Validation (equal); Visualization (equal); Writing – review & editing (equal). Arup Neogi: Data (equal); Writing – review & editing (equal). Arup Iveogr. Data = curation (equal); Formal analysis (equal); Funding acquisition (equal); Investigation (equal); Project administration (equal); Resources (equal); Supervision (equal); Validation (equal); Visualization (equal); Writing – review & editing (equal).

The data that support the findings of this study are available from the corresponding author upon reasonable request.

REFERENCES

- ¹H. Gan, S. P. Nandi, and P. L. Walker, Jr., Fuel 51, 272 (1972).
- ²K. Chandra, Int. J. Geol. **69**, 261 (1997).
- ³B. B. Xodot, S. Z. Song, and Y. A. Wang, Coal and Gas Outburst (China Industry Press, Beijing, 1966), p. 1.
- B. Nie, X. Liu, L. Yang, J. Meng, and X. Li, Fuel 158, 908 (2015).
- ⁵G. Liu, H. Wu, R. P. Gupta, J. A. Lucas, A. G. Tate, and T. F. Wall, Fuel **79**, 627 (2000). ⁶S. Yao, K. Jiao, K. Zhang, W. Hu, H. Ding, M. Li, and W. Pei, Chin. Sci. Bull. 56, 2712 (2011).
- 7K. Christensen-Jeffries, O. Couture, P. A. Dayton, Y. C. Eldar, K. Hynynen, F. Kiessling, and M. O'Reilly, Ultrasound Med. Biol. 46, 865 (2020).
- ⁸M. V. Pantawane, T. Yang, Y. Jin, S. S. Joshi, S. Dasari, A. Sharma, A. Krokhin et al., Sci. Rep. 11, 1 (2021).
- ⁹M. V. Pantawane, T. Yang, Y. Jin, S. Mazumder, M. Pole, S. Dasari, A. Krokhin et al., Mater. Sci. Eng. A 811, 140990 (2021).
- ¹⁰F. Honarvar and A. Varvani-Farahani, Ultrasonics 108, 106227 (2020).
- ¹¹K. M. Meiburger, U. R. Acharya, and F. Molinari, Comput. Biol. Med. 92, 210
- ¹²A. A. Krokhin, J. Arriaga, and L. N. Gumen, *Phys. Rev. Lett.* **91**, 264302 (2003).
- 13Y. Jin, E. Walker, H. Heo, A. Krokhin, T.-Y. Choi, and A. Neogi, Smart Mater. Struct. 29, 045020 (2020).

¹⁴Y. Jin, T. Yang, S. Ju, H. Zhang, T.-Y. Choi, and A. Neogi, Polymers 12, 1462 (2020).

15 D. T. Blackstock, Fundamentals of Physical Acoustics (Wiley-Interscience, 2001).

¹⁶A. D. Pierce and R. T. Beyer, Acoustics: An Introduction to Its Physical Principles and Applications (Springer, 1990).

¹⁷A. Morcote, G. Mavko, and M. Prasad, Geophysics 75, E227, (2010).

¹⁸ Y. Jin, E. Walker, A. Krokhin, H. Heo, T.-Y. Choi, and A. Neogi, IEEE Trans. Ultrason. Ferroelectr. Freq. Control 67, 624 (2020).

19D. Taulbee, S. H. Poe, T. Robl, and B. Keogh, Energy Fuels 3, 662